Theoretical and experimental study of the structural stability of $TbPO_4$ at high pressures

J. López-Solano,[1,*] P. Rodríguez-Hernández,[1] A. Muñoz,[1] O. Gomis,[2] D. Santamaría-Perez,[3] D. Errandonea,[4] F. J. Manjón,[5] R. S. Kumar,[6] E. Stavrou,[7] and C. Raptis[7]

[1]*MALTA Consolider Team, Departamento de Física Fundamental II, Universidad de La Laguna, La Laguna, Tenerife, Spain*

[2]*Centro de Tecnologías Físicas, MALTA Consolider Team, Universitat Politècnica de València, 46022 Valencia, Spain*

[3]*MALTA Consolider Team, Departamento de Química Física I, Universidad Complutense de Madrid, Avenida Complutense s/n, 28040 Madrid, Spain*

[4]*MALTA Consolider Team, Fundación General de la Universitat de València, Edificio de Investigación, C. Dr. Moliner, 50, Burjassot, 46100 Valencia, Spain*

[5]*Instituto de Diseño para la Fabricación y Producción Automatizada, MALTA Consolider Team, Universitat Politècnica de València, 46022 Valencia, Spain*

[6]*High Pressure Science and Engineering Center, Department of Physics and Astronomy, University of Nevada–Las Vegas, 4505 Maryland Parkway, Las Vegas, Nevada 89154-4002, USA*

[7]*Physics Department, National Technical University of Athens, GR-15780 Athens, Greece*

(Received 1 March 2010; published 30 April 2010)

We have performed a theoretical and experimental study of the structural stability of terbium phosphate at high pressures. Theoretical *ab initio* total-energy and lattice-dynamics calculations together with x-ray diffraction experiments have allowed us to completely characterize a phase transition at ~9.8 GPa from the zircon to the monazite structure. Furthermore, total-energy calculations have been performed to check the relative stability of 17 candidate structures at different pressures and allow us to propose the zircon→monazite→scheelite→$SrUO_4$-type sequence of stable structures with increasing pressure. In this sequence, sixfold P coordination is attained for the $SrUO_4$-type structure above 64 GPa. The whole sequence of transitions is discussed in association with the high-pressure structural behavior of oxides isomorphic to $TbPO_4$.

DOI: 10.1103/PhysRevB.81.144126 PACS number(s): 61.05.cp, 61.50.Ks, 62.50.−p, 71.15.Nc

I. INTRODUCTION

The structural behavior of ABO_4 compounds under pressure is a challenging problem with implications in many fields including earth, planetary, and materials sciences.[1] In particular, orthophosphates (APO_4) are relevant in mineral physics and chemistry and very important for petrology studies.[2] Additionally, they have a wide potential for their application in optoelectronics due to their optical and luminescent properties.[3,4] Other interests in these compounds are related to their use as solid-state repository for radioactive waste[5] or for oxidation-resistant ceramic toughening.[6]

Pressure-induced transitions in ABO_4 compounds have been recently reviewed on the light of the most recent experimental and theoretical advances.[7] It has been proved that crystal-chemistry arguments, e.g., the Bastide's diagram,[7] are helpful to understand the ambient pressure phases and pressure-induced phase transitions in ABO_4 compounds. Many zircon-type structures have been studied under pressure and the zircon-scheelite-fergusonite sequence of phase transitions has been observed in many of them when the compounds are close to the zircon-scheelite equilibrium border, as it happens for vanadates and germanates.[8–14] Much less is known about the pressure behavior of zircon-type structures which are far from the zircon-scheelite border, such as phosphates. Recently, a number of zircon-type and monazite-type phosphates have been studied under pressure. The interest on these compounds was partially triggered by the finding of a phase with sixfold coordination for P in $AlPO_4$ at 47 GPa.[15] High-pressure experiments have evidenced that $LuPO_4$, $YbPO_4$, and $ScPO_4$ follow the same structural sequence as the mineral zircon ($ZrSiO_4$) with the zircon-to-scheelite transition occurring beyond 19 GPa.[16,17] However, a zircon-to-monazite transition has been measured in YPO_4 and $ErPO_4$,[18] and the complete zircon-monazite-scheelite sequence has been found in YPO_4.[17] Note that in comparison with tetragonal zircon and scheelite, the monazite structure has a lower monoclinic symmetry. Finally, phosphates crystallizing in the monazite structure, such as $GdPO_4$, $EuPO_4$, $NdPO_4$, and $LaPO_4$, have been studied under pressure.[18] A phase transition was detected only in $LaPO_4$ at 26.4 GPa. All these facts show that additional studies are needed in order to understand the high-pressure behavior of phosphates. In this study we will focus on terbium phosphate ($TbPO_4$).

$TbPO_4$ features an A cation with a large ionic radius, very close to that of other APO_4 compounds such as $GdPO_4$ and YPO_4. It is a compound with tetragonal zircon structure [space group (SG) no. 141, $I4_1/amd$, $Z=4$] at ambient conditions. The zircon structure has A and B cations forming two interpenetrating diamond structures in a tetragonally distorted fcc array and it exhibits AO_8 bisdisphenoid and PO_4 tetrahedra.[19] Depending on the preparation conditions, $TbPO_4$ can also adopt the monoclinic monazite-type structure (SG no. 14, $P2_1/n$, $Z=4$) at ambient pressure.[20] A similar dimorphism pattern has also been displayed by the closely related $GdPO_4$ compound[20] which exhibits a very similar radius for the A cation, but favors crystallization in the monazite structure at ambient conditions. Recent high-pressure Raman measurements on zircon-type $TbPO_4$ have shown that a phase transition occurs at 9.5 GPa and a mono-

clinic structure has been proposed as a high-pressure candidate.[21] Furthermore, based on the similarity between the spectra of the high-pressure phase of $TbPO_4$ and that of the related monazite-type $GdPO_4$ compound at ambient pressure, the authors of Ref. 21 suggested that the most likely candidate for the high-pressure structure of $TbPO_4$ was monazite.

In this work, we study the possible pressure-induced structural phase transitions of $TbPO_4$ theoretically by means of total-energy and lattice-dynamics *ab initio* calculations and also experimentally by means of x-ray diffraction measurements. Our theoretical study extends above the maximum pressure reached in the experiments and further transitions are predicted.

II. THEORETICAL AND EXPERIMENTAL METHODS

A. Calculation details

Our first-principles total-energy and lattice-dynamics calculations have been performed within the framework of the density-functional theory and the pseudopotential method, as implemented in the Vienna *ab initio* simulation package (VASP).[22] Projector-augmented wave[23] pseudopotentials within the generalized gradient approximation (GGA) prescription of the exchange and correlation energy of Perdew, Burke, and Ernzerhof[24] were used. The set of plane waves used in the calculations extended up to a kinetic energy cutoff of 550 eV. The Monkhorst-Pack[25] method, with dense grids appropriate to each structure, was used to perform the integrations in the reciprocal space. With these parameters total energies were converged up to ~ 1 meV/f.u. At each selected volume the structures were fully relaxed to their equilibrium configuration through the calculation of the forces on the atoms and the stress tensor.[26,27] In the relaxed equilibrium configuration the forces were less than 0.004 eV/Å and the deviation of the stress tensor from a diagonal hydrostatic form was less than 1 kbar (0.1 GPa).

These highly converged forces were required for the calculation of the phonon spectra at the Γ point using the direct force constant approach, or supercell, method.[28] In this method, the dynamical matrix is obtained from the calculation of the forces over all the atoms when each one is displaced from its equilibrium configuration independently from the others. Symmetry considerations can be used to reduce the number of such independent distortions. Diagonalization of the dynamical matrix then provides both the frequencies of the normal modes and their polarization vectors and allows to identify the irreducible representation and character of the phonon modes.

B. Experimental details

Single crystals of $TbPO_4$ were grown by the flux method described in Ref. 21. In fact, the crystalline samples used in the present work originated from the same large single crystal as the samples of Ref. 21. Ambient pressure x-ray diffraction and Raman measurements confirmed that the crystals have a zircon-type structure. To perform x-ray powder diffraction measurements crystals were crushed in a mortar to obtain a micron-sized powder. Three independent high-pressure angle-dispersive x-ray diffraction experiments were conducted at room temperature. Experiment 1 was carried out up to 14 GPa with a Xcalibur diffractometer (Oxford Diffraction Ltd.). X-ray diffraction patterns were obtained on a 135 mm Atlas CCD detector placed at 105 mm from the sample using $K\alpha 1:K\alpha 2$ molybdenum radiation. The x-ray beam was collimated to a diameter of 300 μm. The measurements were performed in a modified Merrill-Bassett diamond-anvil cell (DAC) with diamond culets of 500 μm. $TbPO_4$ was loaded in a 160-μm-diameter hole of the stainless-steel gasket preindented to a thickness of 60 μm. A 4:1 methanol:ethanol mixture was used as pressure-transmitting medium. Exposure times were typically of 1 h. The CRYSALIS software (Oxford Diffraction Ltd.) was used for data collection and preliminary data reduction. Experiments 2 and 3, up to 16 GPa and 25 GPa, respectively, were performed at the 16-IDB station of the High Pressure Collaborative Access Team (HPCAT)—Advanced Photon Source (APS) with an incident monochromatic wavelength of 0.40695 Å and 0.37571 Å, respectively. In both experiments, diffraction patterns were collected using a symmetric Mao-Bell-type DAC with diamond-culet sizes of 480 μm and with $TbPO_4$ loaded in a 200 μm hole of a rhenium gasket preindented to a 40 μm thickness. In experiment 2 the pressure-transmitting medium was neon (Ne) and in experiment 3 it was silicone oil. The x-ray beam was focused down to 10×10 μm^2 using Kickpatrick-Baez mirrors. X-ray diffraction images were collected using a MAR345 image plate located at 440 mm away from the sample and then integrated and corrected for distortions using FIT2D. The typical acquisition time was 100 s. In all the experiments the pressure was determined using the ruby fluorescence technique. The indexing and refinement of the powder patterns were performed using the DICVOL and POWDERCELL program packages.

III. RESULTS AND DISCUSSION

A. Ambient pressure and first phase transition

1. Ab initio results

For our theoretical study of the structural stability of $TbPO_4$ at high pressures, we have taken into consideration previous results obtained in the ABX_4 family of compounds and the packing-efficiency criterion proposed by Bastide.[2,29] We have studied the relative stability of 17 high-pressure candidate structures using the calculation method outlined in the previous section. Figure 1 shows a diagram of Bastide with all the structures analyzed in order to understand the pressure-induced phase transitions in rare-earth orthophosphates and, particularly, in $TbPO_4$. The structures located along the north-east (NE) direction with respect to the zircon-type $TbPO_4$ feature a gradual increment of the atomic coordination and are likely high-pressure phases.[30] In the following paragraph we summarize and give some details of these structures. Further details can be found in the references provided or in the Inorganic Crystal Structure Database (ICSD).[31]

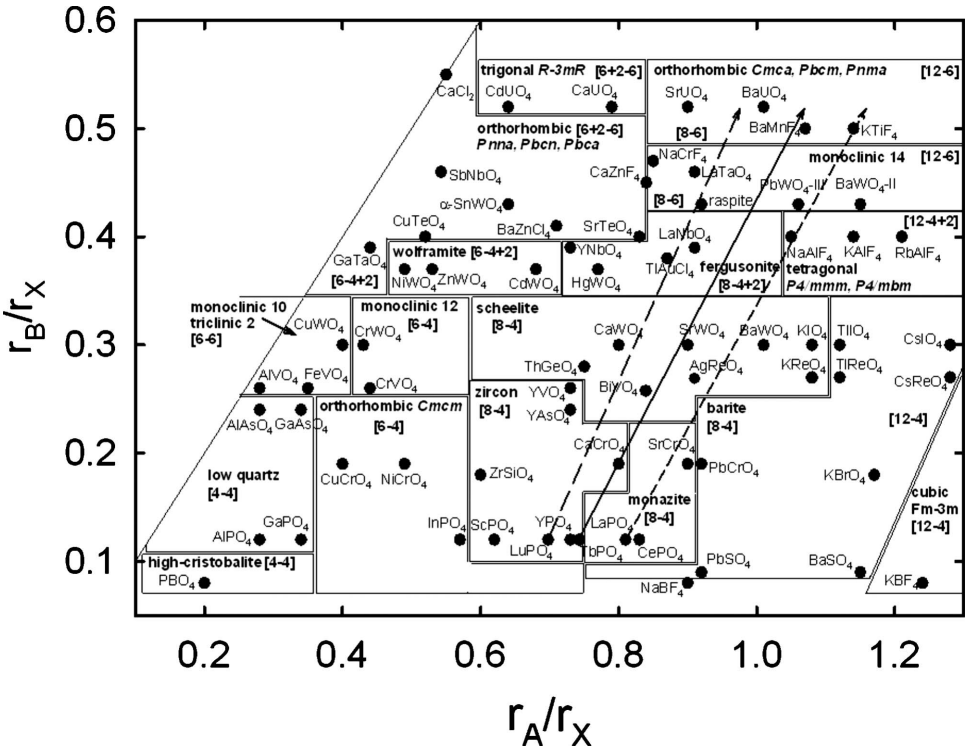

FIG. 1. Bastide's diagram. ABX_4 compounds are represented according to the ionic radii of their elements (r_A, r_B, r_X). The diagram shows relevant compounds for the study of the high-pressure phases of orthophosphates. Shannon's radii have been used to place different compounds in the diagram. The arrows along the NE direction mark the sequence of the pressure-induced phase transitions in rare-earth orthophosphates. It can be observed that there are at least three sequences of phase transitions: (i) zircon-type compounds such as $ScPO_4$, $LuPO_4$, and $YbPO_4$ (dashed line) undergo a phase transition from zircon to scheelite; (ii) zircon-type compounds such as YPO_4, $ErPO_4$, and $TbPO_4$ (solid line) undergo a phase transition from zircon to monazite and afterwards to scheelite; and (iii) monazite-type compounds such as $LaPO_4$, $NdPO_4$, and $CePO_4$ are expected to undergo a phase transition from monazite to scheelite or to barite depending on the closeness of the orthophosphate to the barite border.

$TbPO_4$ can be found in ambient conditions in the zircon (SG no. 141, $I4_1/amd$, $Z=4$) or monazite ($CePO_4$ type, SG no. 14, $P2_1/n$, $Z=4$) structure, depending on the growth conditions. The monazite structure can also be a high-pressure phase in $TbPO_4$ as it occurs for YPO_4 and $ErPO_4$.[17,18] Another possible postzircon phase that has been analyzed is the scheelite structure ($CaWO_4$ type, SG no. 88, $I4_1/a$, $Z=4$). This phase has been found at high pressures in $YbPO_4$, $LuPO_4$, $ScPO_4$, and YPO_4 (in the later case, after monazite).[16,17] Other possible high-pressure phases are the wolframite ($FeWO_4$ type, SG no. 13, $P2/c$, $Z=2$) and $HgWO_4$-type (SG no. 15, $C2/c$, $Z=4$) monoclinic structures. Some high-pressure postscheelite and postwolframite structures have also been considered as potential high-pressure phases in $TbPO_4$, e.g., monoclinic M-fergusonite (SG no. 15, $I2/a$, $Z=4$).[32–35] The barite ($BaSO_4$ type, SG no. 62, *Pnma*, $Z=4$) structure has also been included in our study because it has been observed in $CaSO_4$ (Ref. 36) and $LaPO_4$ (Ref. 18) as a postmonazite phase. The m-$CaCl_2$ (SG no. 10, $P2/m$, $Z=1$) and $CrVO_4$-type (SG no. 63, *Cmcm*, $Z=4$) structures have been analyzed because both have been observed in $AlPO_4$,[15] but their location in Bastide's diagram do not make them likely stable structures for $TbPO_4$. The $CrVO_4$ structure has also been found in zircon-related silicates such as $TiSiO_4$.[37] Other possible postmonazite and postbarite phases analyzed are the $NaAlF_4$-type (SG no. 123, $P4/mmm$, $Z=1$) and $KAlF_4$-type (SG no. 127, $P4/mbm$, $Z=2$) structures, which according to Fig. 1 are candidate postmonazite structures. Finally, phases with large cation coordination have been considered, like the $BaWO_4$-II-type structure (SG no. 14, $P2_1/n$, $Z=8$),[38] and several orthorhombic structures: $CaUO_4$-type (SG no. 166, $R\text{-}3m$, $Z=1$); $SrUO_4$-type (SG no. 57, *Pbcm*, $Z=4$); $BaMnF_4$-type (SG no. 36, $A2_1am$, $Z=4$); $BaZnCl_4$-type (SG no. 60, *Pbcn*, $Z=4$); and Cmca (SG no. 64, *Cmca*, $Z=8$). All of them can be plausible high-pressure structures of $TbPO_4$ according to packing-efficiency arguments, and some of them have been found to be energetically competitive at extreme pressures in ABX_4 compounds.[33,38]

Figure 2 shows the energy as a function of volume curves for all the calculated structures, except for the M-fergusonite structure. After performing a full optimization of the lattice parameters and atomic positions, we found that this structure was indistinguishable both energetically and structurally from the scheelite in all the volume range considered. Our theoretical study indicates that zircon is the structure of $TbPO_4$ with the lowest enthalpy at ambient pressure. A fit with a Birch-Murnaghan fourth-order equation of state (EOS) (Ref. 39) gives values in good agreement with experimental results presented in the next section, as shown in Table I. The equilibrium volume V_0 is overestimated by $\sim 2\%$, as usual with the GGA approximation,[40] and in turn the bulk modulus B_0 is underestimated by a similar propor-

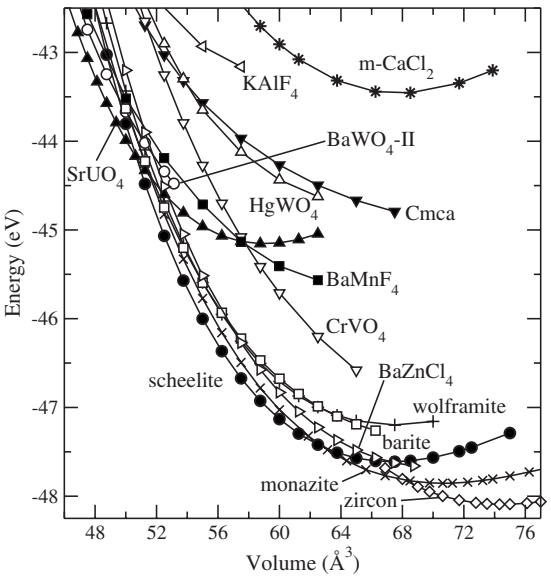

FIG. 2. Energy as a function of volume curves for the zircon (◇), monazite (×), scheelite (●), $SrUO_4$-type (▲), $BaZnCl_4$-type (▷), barite (□), wolframite (+), $CrVO_4$-type (▽), $BaMnF_4$-type (■), $BaWO_4$-II-type (○), $HgWO_4$-type (△), Cmca (▼), $KAlF_4$-type (◁), and m-$CaCl_2$ (∗) structures. Energy and volume are written per formula unit.

tion: 4.5% with respect to the experimental value obtained with a nonfixed first derivative of the bulk modulus B'_0 (see the next section). In Ref. 17, the experimental and theoretical bulk moduli of the YPO_4 compound show the same difference. Full structural information of the zircon structure is provided in Table II, and it also shows a good agreement between theory and experiment.

Table III shows a comparison between the ambient-pressure Raman spectra measured by Tatsi *et al.*[21] and the one calculated in this work. There is a reasonable agreement between experimental and theoretical values, although the theoretical frequencies are lower in general. This may be related to the use of the GGA approximation in the calculations.[41] The most noticeable difference is the identification in this work of the 12th Raman mode, which was missing in Ref. 21. In our calculations, this mode is classified as B_{1g} with a frequency of 288 cm^{-1}. Given the overall shift of the experimental frequencies with respect to the theoretical ones, the peak corresponding to this mode should be

TABLE I. *Ab initio* and experimental (in brackets) equilibrium volume V_0, bulk modulus B_0, and its first derivative B'_0 of the zircon, monazite, scheelite, and $SrUO_4$-type structures. Two sets of experimental values are given for zircon, (a) with B'_0 fixed at a value of 4 and (b) with B'_0 nonfixed. These data were obtained from experiment 2.

	Zircon	Monazite	Scheelite	$SrUO_4$ type
V_0 (Å^3)	298 (291.4 (a), 291.4 (b))	283 (277)	269	236
B_0 (GPa)	128 (144 (a), 134 (b))	119 (152)	152	196
B'_0	6.1 (4 (a), 6.4 (b))	6.4 (4)	5.8	5.0

TABLE II. *Ab initio* and experimental parameters of the zircon structure (SG no. 141, $I4_1/amd$) at ambient pressure.

	Ab initio	Experiment 1
a (Å)	6.9913	6.9391(3)
c (Å)	6.0823	6.0694(3)
V (Å^3)	297.29	292.25
Tb	0, 0.75, 0.125	0, 0.75, 0.125
P	0, 0.25, 0.375	0, 0.25, 0.375
O	0, 0.0761, 0.2157	0, 0.0775(6), 0.2138(7)

located at ~300 cm^{-1} in the experimental Raman spectra, where it would be difficult to distinguish from the closely located E_g and B_{2g} modes (see Fig. 1 in Ref. 21).

Upon increasing the pressure, major changes in the Raman spectra of $TbPO_4$ starting at 9.5 GPa were reported in Ref. 21. This marks a first-order phase transition to a structure which could not be fully identified by Tatsi *et al.* However, on the basis of the large number of Raman modes observed and the similarity of the high-pressure spectra of $TbPO_4$ to the ambient conditions spectrum of monazite-structure $GdPO_4$, these authors proposed a monoclinic structure as the high-pressure phase of $TbPO_4$ and suggested that, most likely, it was the monazite structure. Our calculations fully support this hypothesis, because monoclinic monazite is the structure with the lowest enthalpy after the zircon phase. The calculated enthalpy as a function of pressure curves shown in Fig. 2 indicate a zircon-to-monazite transition pressure of 9.6 GPa, which is in excellent agreement with the experimental value of Ref. 21 and our own diffraction experiments (see the next section).

According to group-theory considerations, the monazite structure has the 36 Raman-active modes summarized in Table IV, where the experimental and theoretical frequencies are compared. We have attempted to identify the symmetry

TABLE III. Comparison of *ab initio* and experimental (from Ref. 21) Raman modes in the zircon structure at ambient pressure.

	Ab initio		Experiment	
Raman mode	ω (cm^{-1})	$\partial\omega/\partial P$ (cm^{-1}/GPa)	ω (cm^{-1})	$\partial\omega/\partial P$ (cm^{-1}/GPa)
E_g	126	0.033	130	−0.070
B_{1g}	137	1.157	141	1.025
E_g	178	0.137	185	0.100
E_g	276	4.667	293	3.920
B_{1g}	288	2.341		
B_{2g}	314	−0.505	331	−0.560
A_{1g}	463	1.082	484	0.720
E_g	548	1.163	576	1.100
B_{1g}	620	2.098	649	1.980
A_{1g}	948	5.329	995	5.300
E_g	969	5.172	1014	5.000
B_{1g}	1006	5.589	1049	5.300

TABLE IV. Comparison of the 36 *ab initio* and experimental (Ref. 21) Raman frequencies ω (cm^{-1}) and slopes $\partial\omega/\partial P$ (cm^{-1}/GPa) for the monazite structure at ~10 GPa. Note that only the values of the frequencies and slopes are given in Ref. 21, the mode assignment corresponds to this work.

	Ab initio		Experiment	
Mode	ω	$\partial\omega/\partial P$	ω	$\partial\omega/\partial P$
B_g	80	−0.46		
A_g	90	0.54		
A_g	113	0.47	114	0.19
A_g	129	0.64		
B_g	135	0.71		
B_g	144	0.68	141	0.32
B_g	155	0.40		
A_g	176	−0.77	173	−0.27
B_g	197	2.30		
A_g	206	1.15		
A_g	211	2.63	205	2.32
A_g	258	2.43	235	2.12
B_g	261	3.17	271	3.82
B_g	271	2.62	283	1.19
A_g	294	3.65		
B_g	298	2.58	314	1.47
B_g	320	3.13		
A_g	330	2.17	337	2.40
B_g	406	2.44	379	0
A_g	430	2.20	420	0.66
A_g	476	2.13	454	2.19
A_g	520	0.73	497	1.10
B_g	522	2.10		
B_g	551	1.23	543	0.34
A_g	565	1.62		
B_g	587	1.60	593	1.30
A_g	619	1.29	616	0.95
B_g	623	1.43	645	1.01
B_g	968	3.58		
A_g	980	3.47	984	4.71
A_g	1005	3.98	1014	0.42
A_g	1033	4.08	1033	2.37
B_g	1040	3.55		
A_g	1070	3.81		
B_g	1080	3.77		
B_g	1093	4.09		

of the experimental modes by comparing the experimental and theoretical values of the frequencies and pressure coefficients. While there are cases in which it is not possible to match the experimental and *ab initio* frequencies and slopes, the overall agreement is reasonable. Note that although Tatsi *et al.*[21] did not observe modes above 1033 cm^{-1}, Silva *et al.*[42] measured modes up to 1091 cm^{-1} in the related compound $GdPO_4$, in agreement with the high frequencies calculated in this work. However, even in their polarized Raman measurements in various monazites Silva *et al.* were only able to observe 22 modes. This is in agreement with the measurements of Tatsi *et al.* This result can be understood if we consider the very small scattering efficiencies of some modes and the possible degeneracy of many Raman modes forming doublets due to the small splitting of many A_g and B_g modes deriving from zircon-type E_g modes (see Table IV). Silva *et al.* found five monazite-type modes above 970 cm^{-1} corresponding to internal ν_1 and ν_3 modes of the PO_4 tetrahedron. However, in high-pressure $TbPO_4$, Tatsi *et al.* observed only three modes. These facts contrast with the eight modes predicted by our calculations above 968 cm^{-1}. New Raman experiments under compression are needed to clarify these apparent discrepancies.

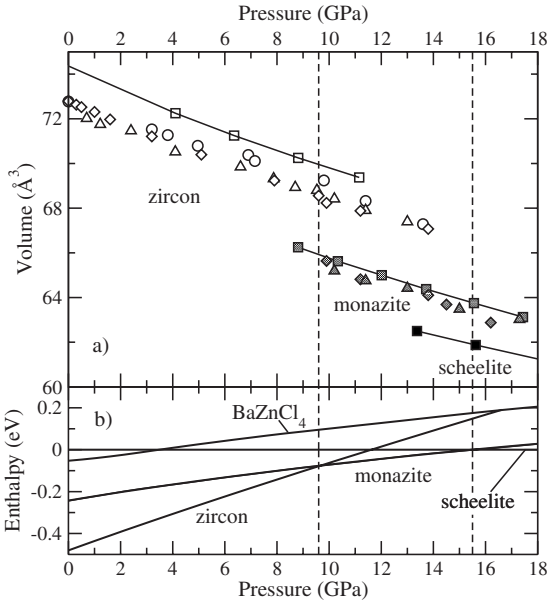

FIG. 3. (a) Volume as a function of pressure and (b) enthalpy as a function of pressure curves for pressures up to 18 GPa. Theoretical data are represented by squares, experiment 1 data by circles, experiment 2 by diamonds, and experiment 3 by triangles. White symbols correspond to the zircon structure, gray to monazite, and black to scheelite. Vertical dashed lines mark the theoretical zircon-to-monazite and monazite-to-scheelite transition pressures of 9.6 GPa and 15.5 GPa, respectively. In (b) the enthalpy is measured with respect to the enthalpy of the scheelite structure at each pressure. Volume and enthalpy are written per formula unit.

From Fig. 3, in the theoretical zircon-to-monazite first-order phase transition there is a volume change of a 6%. Table I shows that there is a difference of only 2% between our theoretical and experimental equilibrium volumes, but a large difference of ~28% between both bulk moduli. This difference can be attributed to the GGA approximation and to the lack of enough experimental data to perform an EOS fit with a nonfixed B'_0. Note that Zhang *et al.*[17] also found a similar difference between the theoretical and experimental bulk moduli of the monazite structure of YPO_4. As shown in Table V, the theoretical and experimental parameters of the monazite structure are in agreement. In the zircon-to-monazite transition the Tb coordination increases from 8 to

TABLE V. *Ab initio* and experimental parameters of the monazite structure (SG no. 14, $P2_1/n$, $Z=4$).

	Ab initio	Experiment 1	Experiment 2
P (GPa)	10.3	13.6	14.5
a (Å)	6.49	6.50(4)	6.38(1)
b (Å)	6.702	6.63(4)	6.58(1)
c (Å)	6.212	6.17(4)	6.11(1)
β (deg)	103.78	103.7(8)	101.0(7)
V (Å^3)	262.5	258(6)	251.8(9)
Tb	0.284, 0.152, 0.094	0.282, 0.155, 0.097	0.288, 0.159, 0.096
P	0.302, 0.160, 0.611	0.303, 0.161, 0.613	0.317, 0.167, 0.612
O_1	0.248, 0.001, 0.436	0.254, 0.001, 0.438	0.263, 0.016, 0.420
O_2	0.385, 0.341, 0.504	0.384, 0.335, 0.502	0.400, 0.356, 0.520
O_3	0.477, 0.105, 0.820	0.473, 0.102, 0.813	0.492, 0.119, 0.805
O_4	0.116, 0.211, 0.720	0.119, 0.214, 0.713	0.101, 0.226, 0.736

8+1, but the P coordination remains the same, with four O neighbors at distances between 1.53 and 1.55 Å, and the next ones at distances of ~3 Å.

To conclude this section, we note that in Ref. 21 the scheelite-type structure was also considered as a possible second stable phase of $TbPO_4$, although it was discarded because its number of Raman modes is incompatible with the measured spectra. In our calculations, the scheelite structure is fairly close in enthalpy to the monazite structure, and indeed the stability range of the latter is rather small because it becomes unstable with respect to the former. We discuss this transition in Sec. III B.

2. Experimental results

Figure 4 shows a selection of diffraction patterns measured in experiment 2. It can be seen that up to 9.6 GPa the only change in the diffraction patterns is the shift of the Bragg peaks due to the unit-cell volume reduction induced by pressure. Indeed all the diffraction patterns collected in this pressure range can be properly indexed with the zircon structure. At 9.9 GPa, additional peaks are detected. Upon further compression, the intensity of these peaks increases whereas that of the zircon peaks decreases. At 14.5 GPa all the peaks of the zircon phase have disappeared. These facts indicate that the onset of a phase transition is detected at 9.9 GPa with the low- and high-pressure phases coexisting in the region of 9.9–13.8 GPa. Upon further compression there is no evidence of an additional transition or decomposition in the sample up to the maximum pressure of 16 GPa reached in experiment 2. Upon decompression the transition appeared to be fully reversible with a very small hysteresis.

Similar results were obtained in the other two experiments. In experiment 3 the onset of the transition was detected at 10.2 GPa and the low- and high-pressure phases were found to coexist up to 15 GPa. Diffraction patterns with only the high-pressure phase were collected from 15.5 to 25 GPa. In this experiment the transition was irreversible and a mixture of the zircon and monazite structures are recovered at ambient pressure. In experiment 1, the transition was detected at 9.8 GPa, and both phases coexisted up to 13.6 GPa, where the zircon peaks were still present but were very weak. In this experiment the transition was also irreversible. Small differences among experiments can be caused by the different hydrostaticity environments used. It is also important to note that in experiments 2 and 3 some strong preferred orientation along the (011) direction was present in the high-pressure phase. As a consequence, the intensity of the

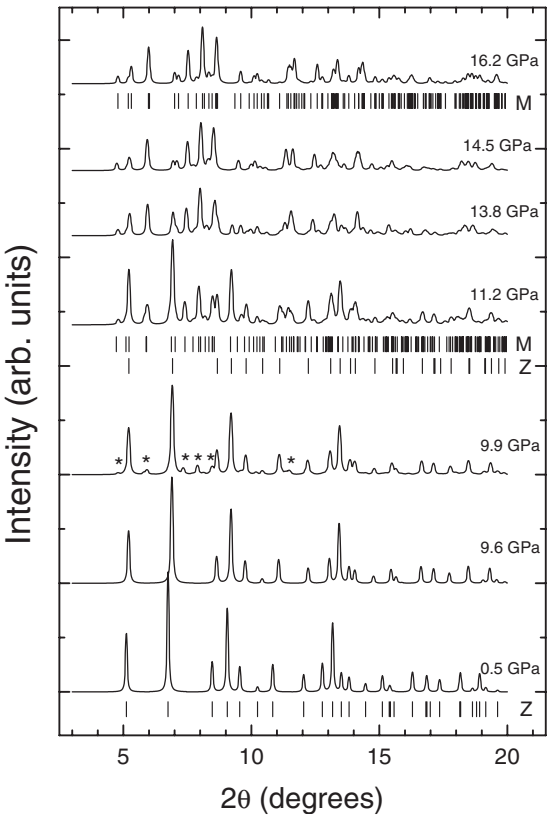

FIG. 4. Selected x-ray diffraction patterns collected in $TbPO_4$ using neon as pressure-transmitting-medium (experiment 2). The stars indicate the most relevant peaks of the high-pressure phase that can be identified at 9.9 GPa. Ticks indicate the calculated Bragg reflections in zircon (z) and monazite (m).

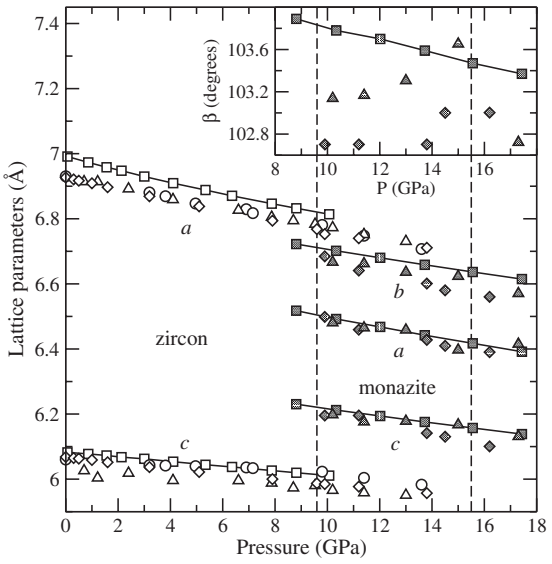

FIG. 5. Evolution of the zircon and monazite lattice parameters with pressure according to our *ab initio* (squares) and experimental (experiment 1: circles; experiment 2: diamonds; and experiment 3: triangles) data. White symbols correspond to the zircon structure, gray ones to the monazite. The inset shows the pressure dependence of the monazite beta angle. Vertical dashed lines mark the theoretical transition pressures.

(200) peak of monazite was much smaller than expected. However, this does not preclude the identification of the high-pressure phase as monazite.

A Rietveld refinement of the patterns collected for the zircon phase in different experiments allowed us to obtain the pressure evolution of the lattice parameters of the low-pressure phase. The results are summarized in Fig. 5. As it also happens in other zircon-structured phosphates[10,13,18] the compression of the unit cell is slightly nonisotropic, increasing the c/a axial ratio upon compression from 0.874 at ambient pressure to 0.892 at 13.6 GPa. We also extracted the pressure evolution of the unit-cell volume, summarized in Fig. 3. Analyzing these data with a second- and third-order Birch-Murnaghan EOS we obtained the parameters summarized in Table I. The three experiments show a similar axial and bulk compressibility. The agreement with calculations is also good. The calculations gave a slightly smaller bulk modulus but similar differences have been found in other zircon-structured compounds. For example, in YPO_4 the experimental bulk modulus is 186 GPa whereas theory predicts $B_0=165$ GPa.[17,18] Note that among all the studied zircon-type phosphates[18] $TbPO_4$ is the one with the smallest bulk modulus. Since in these compounds the volume change is basically accounted for by that of the TbO_8 units, this observation is consistent with the fact that $TbPO_4$ has the largest AO_8 bisdisphenoids among APO_4 phosphates.

Previous studies have found that zircon-type phosphates tend to transform upon compression either to the scheelite or monazite structure. Our calculations predict the zircon-monazite transition to take place at 9.6 GPa. A Rietveld refinement of the spectra collected for the high-pressure phase of $TbPO_4$ confirms that this phase has a monazite-type structure. The lattice parameters and atomic positions obtained for this phase are summarized in Table V. There is a marked volume reduction of about 3.5% at the transition, which indicates its first-order character. Similar volume changes have been detected at this transition in YPO_4 and $ErPO_4$.[18] As observed in the zircon phase, the compression of the monazite phase is also anisotropic. In particular, the most compressible axis is the a axis. In the experiments, for the β monoclinic angle we obtained a scatter of data as a function of pressure. However, the calculations indicate that β decreases upon compression. This decrease is consistent with what has been experimentally observed for the monazite structure in the $LaPO_4$, $NdPO_4$, $EuPO_4$, and $GdPO_4$ compounds.[18]

TABLE VI. *Ab initio* parameters of the scheelite (SG no. 88, $I4_1/a$, $Z=4$) and $SrUO_4$-type (SG no. 57, *Pbcm*, $Z=4$) structures.

	Scheelite	$SrUO_4$ type
P (GPa)	20.5	77.1
a (Å)	4.724	4.621
b (Å)		6.355
c (Å)	10.867	6.384
V (Å^3)	242.5	187.5
Tb	0, 0.25, 0.625	0.472, 0.192, 0.25
P	0, 0.25, 0.125	0, 0, 0
O_1	0.243, 0.124, 0.0486	0.698, 0.419, 0.065
O_2		0.140, 0.25, 0
O_3		0.885, 0.023, 0.25

B. Ab initio predictions for further phase transitions

As shown in the enthalpy as a function of pressure curves of Fig. 3, scheelite becomes more stable than monazite at 15.5 GPa, after a first-order transition in which the volume change is about 3%. Although in our experiments we reached a maximum pressure of 25 GPa, kinetic-energy barriers may hinder the transition to the scheelite structure, so that even a higher pressure (or a combination of pressure and temperature) would be necessary to observe this transition in the laboratory. A similar situation was found in Ref. 17, in which the monazite-to-scheelite transition of YPO_4 was experimentally observed at 32 GPa, but *ab initio* calculations predicted a transition pressure of only 20.8 GPa. It should also be noted that a high-pressure scheelite structure has been observed in other phosphates such as $YbPO_4$ and $LuPO_4$,[16] and $ScPO_4$.[17] Furthermore, as shown in Fig. 1, Bastide's diagram also supports the zircon→monazite→scheelite sequence on the basis of the NE rule.

Structural data of the scheelite structure is shown in Table VI. There is a slight decrease in the Tb coordination in the monazite-to-scheelite transition from 8+1 to 8, which is, however, accompanied by an overall shortening of the Tb-O bond lengths. In the scheelite structure there are still four P-O bond lengths of 1.54 Å with the next O neighbors at distances above ~3 Å, and thus the environment of the P cation almost does not change even at these high pressures. This has been attributed to the strong covalent character of

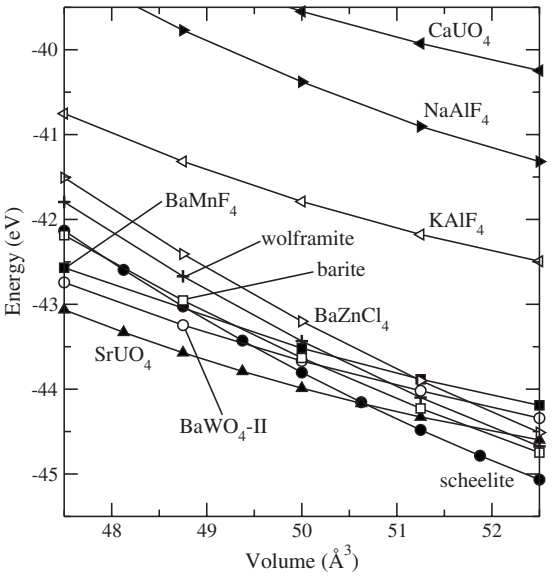

FIG. 6. Same as Fig. 2, but showing in detail the range of more compressed volumes. The structures shown are $SrUO_4$ type (▲), $BaWO_4$-II type (○), scheelite (●), $BaMnF_4$ type (■), barite (□), wolframite (+), $BaZnCl_4$ type (▷), $KAlF_4$ type (◁), $NaAlF_4$ type (▶), and $CaUO_4$-type (◀).

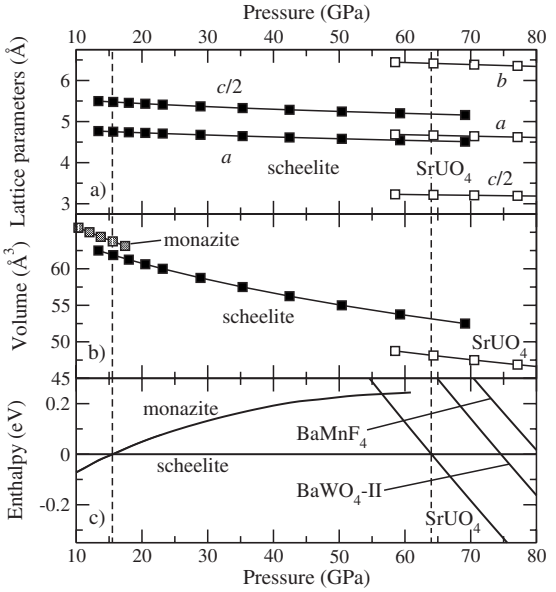

FIG. 7. (a) Calculated pressure evolution of the lattice parameters of the scheelite (black symbols) and $SrUO_4$-type (white symbols) structures, (b) volume as a function of pressure, and (c) enthalpy as a function of pressure (the enthalpy is measured with respect to that of the scheelite structure.). The vertical dashed lines mark the theoretical monazite-to-scheelite and scheelite-to-$SrUO_4$-type transition pressures of 15.5 GPa and 64 GPa, respectively.

these bonds in previous works (see Ref. 15 and references therein). As in the case of $AlPO_4$, very high pressures may be needed to produce the changes in the atomic positions which lead to a higher coordination for P.

The wolframite, $BaWO_4$-II-type, $BaMnF_4$-type, $CaUO_4$-type, $BaZnCl_4$-type, $NaAlF_4$-type, $KAlF_4$-type, and $SrUO_4$-type structures feature sixfold coordination for the P cation and are all located in the NE direction with respect to the zircon structure in the diagram of Bastide. The energy as a function of volume curves of these structures is presented in Fig. 6 and shows that the most competitive are the $BaMnF_4$ type, $BaWO_4$-II type, and $SrUO_4$ type. From the enthalpy as a function of pressure curves in Fig. 7 it can be seen that the $SrUO_4$-type structure, with *Pbcm* symmetry, becomes more stable than the scheelite at a pressure of 64 GPa, after a first-order phase transition with 9% change in the volume.

Full structural data of the $SrUO_4$-type structure of $TbPO_4$ is provided in Table VI. The structure is orthorhombic and belongs to the $n=1$ Dion-Jacobson structures.[43] The Sr atoms (Tb in our case) ions are sandwiched between infinite UO_6 (PO_6) sheets.[44] It can be basically seen as a structure made of perovskitelike slabs separated by Tb cations. At pressures where it is stable, the structure features Tb in 9+1 coordination and PO_6 units in octahedral coordination, with two P-O bond lengths of 1.55 Å, two of 1.69 Å, and another two of 1.72 Å, the next neighbors being at distances above 3 Å. The PO_6 octahedron is thus distorted with a short axial distance of 3.1 Å and two long equatorial distances with an average length of 3.41 Å. It should be noted that the m-$CaCl_2$ structure, found stable above 46.3 GPa in $AlPO_4$, features the same coordination and similar average bond length for P cation.[17]

IV. CONCLUDING REMARKS

In this work we have studied both theoretically and experimentally the stability of the zircon-type phase of $TbPO_4$ and its high-pressure phases. Based on our *ab initio* calculations and crystal-chemical arguments we propose a first phase transition from the zircon to monazite structures at 9.6 GPa in agreement with the suggestions of a previous high-pressure Raman study,[21] followed by a transition to the scheelite structure at 15.5 GPa, and a further one to the $SrUO_4$-type structure at 64 GPa. The zircon and monazite structures are in good agreement with previous studies and also with our own experimental results. Although only a limited set of structures have been considered in our *ab initio* calculations, a stable scheelite phase is supported on the basis of the behavior of similar phosphates. Furthermore, $TbPO_4$ seems to have the same structural phase transitions as those observed in YVO_4 and $ErPO_4$, which are zircon-type compounds with similar rare-earth ionic radii. The stability of the $SrUO_4$-type structure shows that sixfold coordinated phosphorous is more stable than fourfold coordinated P at very high pressures. However, it should be noted that amorphization or chemical decomposition may take place before reaching this range of pressures. In our three experiments we have proved by x-ray diffraction that the zircon-to-monazite phase transition occurs above 10 GPa on average and that the monazite phase seems to be stable up to 25 GPa. Further high-pressure experiments ensuring hydrostatic conditions beyond 30 GPa will be needed to fully confirm our theoretical predictions for the scheelite and $SrUO_4$-type phases.

ACKNOWLEDGMENTS

We acknowledge the financial support of the Spanish MCYT under Grant Nos. MAT2007-65990-C03-01/03 and CSD2007-00045, and the computation time provided by the Red Española de Supercomputación at the supercomputer Atlante. F.J.M. and O.G. acknowledge financial support from Vicerrectorado de Innovación y Desarrollo, UPV (Project No. UPV2008-0020).

*Corresponding author; javierl@marengo.dfis.ull.es

[1] F. J. Manjón and D. Errandonea, Phys. Status Solidi B **246**, 9 (2009).
[2] D. Rubatto, J. Hermann, and I. S. Buick, J. Petrol. **47**, 1973 (2006).
[3] U. Kolitsch and D. Holtstam, Eur. J. Mineral. **16**, 117 (2004).
[4] A. A. Kaminskii M. Bettinelli, A. Speghini, H. Rhee, H. J. Eichler, and G. Mariotto, Laser Phys. Lett. **5**, 367 (2008).
[5] H. Li, S. Zhang, S. Zhou, and X. Cao, Inorg. Chem. **48**, 4542 (2009).
[6] R. S. Hay, Ceram. Eng. Sci. Proc. **21**, 203 (2000).
[7] D. Errandonea and F. J. Manjón, Prog. Mater. Sci. **53**, 711 (2008).
[8] R. Mittal, A. B. Garg, V. Vijayakumar, S. N. Achary, A. K. Tyagi, B. K. Godwal, E. Busetto, A. Lausi, and S. L. Chaplot, J. Phys.: Condens. Matter **20**, 075223 (2008).
[9] J. López-Solano, P. Rodríguez-Hernández, and A. Muñoz, High Press. Res. **29**, 582 (2009).
[10] D. Errandonea, R. Lacomba-Perales, J. Ruiz-Fuertes, A. Segura, S. N. Achary, and A. K. Tyagi, Phys. Rev. B **79**, 184104 (2009).
[11] A. B. Garg, R. Rao, T. Sakuntala, B. N. Wani, and V. Vijayakumar, J. Appl. Phys. **106**, 063513 (2009).
[12] F. J. Manjón, P. Rodríguez-Hernández, A. Muñoz, A. H. Romero, D. Errandonea, and K. Syassen, Phys. Rev. B **81**, 075202 (2010).
[13] D. Errandonea, R. S. Kumar, L. Gracia, A. Beltrán, S. N. Achary, and A. K. Tyagi, Phys. Rev. B **80**, 094101 (2009).
[14] R. Rao, T. Sakuntala, S. N. Achary, and A. K. Tyagi, J. Appl. Phys. **106**, 123517 (2009).
[15] J. Pellicer-Porres, A. M. Saitta, A. Polian, J. P. Itié, and M. Hanfland, Nat. Mater. **6**, 698 (2007).
[16] F. X. Zhang, M. Lang, R. C. Ewing, J. Lian, Z. W. Wang, J. Hu, and L. A. Boatner, J. Solid State Chem. **181**, 2633 (2008).
[17] F. X. Zhang, J. W. Wang, M. Lang, J. M. Zhang, R. C. Ewing, and L. A. Boatner, Phys. Rev. B **80**, 184114 (2009).
[18] R. Lacomba-Perales, D. Errandonea, Y. Meng, and M. Bettinelli, Phys. Rev. B **81**, 064113 (2010).
[19] Y. X. Ni, J. M. Hughes, and A. N. Mariano, Am. Mineral. **80**, 21 (1995).
[20] S. V. Ushakov, K. B. Helean, A. Navrotsky, and L. A. Boatner, J. Mater. Res. **16**, 2623 (2001).
[21] A. Tatsi, E. Stavrou, Y. C. Boulmetis, A. G. Kontos, Y. S. Raptis, and C. Raptis, J. Phys.: Condens. Matter **20**, 425216 (2008).
[22] G. Kresse, J. Hafner, and J. Furthmüller, computer code VASP. Available at http://cms.mpi.univie.ac.at/vasp
[23] P. E. Blöchl, Phys. Rev. B **50**, 17953 (1994).
[24] J. P. Perdew, K. Burke, and M. Ernzerhof, Phys. Rev. Lett. **77**, 3865 (1996).
[25] H. J. Monkhorst and J. D. Pack, Phys. Rev. B **13**, 5188 (1976).
[26] O. H. Nielsen and R. M. Martin, Phys. Rev. Lett. **50**, 697 (1983).
[27] G. Kresse and J. Furthmüller, Phys. Rev. B **54**, 11169 (1996).
[28] K. Parlinski, computer code PHONON. Available at http://wolf.ifj.edu.pl/phonon
[29] F. J. Manjón, D. Errandonea, J. López-Solano, P. Rodríguez-Hernández, S. Radescu, A. Mujica, A. Muñoz, N. Garro, J. Pellicer-Porres, A. Segura, Ch. Ferrer-Roca, R. S. Kumar, O. Tschauner, and G. Aquilanti, Phys. Status Solidi B **244**, 295 (2007).
[30] J. P. Bastide, J. Solid State Chem. **71**, 115 (1987).
[31] G. Bergerhoff and I. D. Brown, in *Crystallographic Databases*, edited by F. H. Allen, G. Bergerhoff, and R. Sievers (International Union of Crystallography, Chester, 1987); A. Belsky, M. Hellenbrandt, V. L. Karen, and P. Luksch, Acta Crystallogr., Sect. B: Struct. Sci. **58**, 364 (2002).
[32] J. López-Solano, P. Rodríguez-Hernández, S. Radescu, A. Mujica, A. Muñoz, D. Errandonea, F. J. Manjón, J. Pellicer-Porres, N. Garro, A. Segura, Ch. Ferrer-Roca, R. S. Kumar, O. Tschauner, and G. Aquilanti, Phys. Status Solidi B **244**, 325 (2007).
[33] J. López-Solano, P. Rodríguez-Hernández, A. Muñoz, and F. J. Manjón, Phys. Rev. B **73**, 094117 (2006).
[34] D. Errandonea, F. J. Manjón, N. Garro, P. Rodríguez-Hernández, S. Radescu, A. Mujica, A. Muñoz, and C. Y. Tu, Phys. Rev. B **78**, 054116 (2008).
[35] R. Lacomba-Perales, D. Errandonea, D. Martínez-García, P. Rodríguez-Hernández, S. Radescu, A. Mújica, A. Muñoz, J. C. Chervin, and A. Polian, Phys. Rev. B **79**, 094105 (2009).
[36] W. A. Crichton, J. B. Parise, S. M. Antao, and A. Grzechnik, Am. Mineral. **90**, 22 (2005).
[37] L. Gracia, A. Beltrán, and D. Errandonea, Phys. Rev. B **80**, 094105 (2009).
[38] D. Errandonea, J. Pellicer-Porres, F. J. Manjón, A. Segura, Ch. Ferrer-Roca, R. S. Kumar, O. Tschauner, J. López-Solano, P. Rodríguez-Hernández, S. Radescu, A. Mujica, A. Muñoz, and G. Aquilanti, Phys. Rev. B **73**, 224103 (2006).
[39] F. Birch, Phys. Rev. **71**, 809 (1947).
[40] A. Mujica, A. Rubio, A. Muñoz, and R. J. Needs, Rev. Mod. Phys. **75**, 863 (2003).
[41] F. Favot and A. Dal Corso, Phys. Rev. B **60**, 11427 (1999).
[42] E. N. Silva, A. P. Ayala, I. Guedes, C. W. A. Paschoal, R. L. Moreira, C.-K. Loong, and L. A. Boatner, Opt. Mater. **29**, 224 (2006).
[43] M. Dion, M. Ganne, and M. Tournoux, Mater. Res. Bull. **16**, 1429 (1981).
[44] T. L. Cremers, P. G. Eller, and E. M. Larson, Acta Crystallogr., Sect. C: Cryst. Struct. Commun. **42**, 1684 (1986).